NASA Contractor Report 189120
MTI Report 91TR56

Heat Pipe Fatigue Test Specimen Metallurgical Evaluation

Steven E. Walak and Michael J. Cronin
Mechanical Technology Incorporated
Latham, New York

Toni Grobstein
NASA-Lewis Research Center
Cleveland, Ohio

January 1992

Prepared for
Lewis Research Center
Under Contract NAS3-25463

NASA
National Aeronautics and
Space Administration

NASA Contractor Report 189120
MTI Report 91TR56

Heat Pipe Fatigue Test Specimen Metallurgical Evaluation

Steven E. Walak and Michael J. Cronin
Mechanical Technology Incorporated
Latham, New York

Toni Grobstein
NASA-Lewis Research Center
Cleveland, Ohio

January 1992

Prepared for
Lewis Research Center
Under Contract NAS3-25463

National Aeronautics and
Space Administration

TABLE OF CONTENTS

LIST OF FIGURES

LIST OF TABLES

LIST OF SYMBOLS

CTPC	Component test power converter
EDM	Electro discharge machining
HPFTS	Heat pipe fatigue test specimen
hr	Hour
Hz	Hertz
in.	Inch
K	Degree kelvin
KHN	Knoop hardness number
ksi	Pounds per square inch × 1000
min	Minute(s)
mm	Millimeters
MPa	Megapascal
Pa	Pascal
ppm	Parts per million
TIG	Tungsten inert gas
W/cm^2	Watt per square centimeter
WDS	Wavelength dispersive x-ray spectrum
°F	Degree fahrenheit
µin.	Microinch (1×10^{-6} inch)
µm	Micrometer (1×10^{-6} meter)

SUMMARY

A sodium-charged Inconel 718 heat pipe with an Ni-200 screen wick was operated for 1090 hr at temperatures between 950 K (1250°F) and 1050 K (1430°F) while being subjected to a mean tensile stress of (21 ksi) and a cyclic tensile stress of ±34 MPa (5 ksi). The heat pipe survived the thermal-mechanical testing sequence and was then sectioned for metallographic and electron microprobe examination. The examination revealed only minor changes in the surface topography and chemistry of the sodium-exposed Inconel 718. Stress-accelerated corrosion, stress corrosion cracking, extensive grain boundary attack and liquid metal embrittlement were not observed.

A surface layer depleted in Cr, Nb, Ti, and Al was formed on the Inconel 718 in all sodium-exposed regions of the heat pipe. Fe and Mo concentrations were also reduced slightly in the condenser. In contrast to previous studies [4], the Ni concentration at the surface of the heart pipe increased as a result of sodium exposure. Chemical interaction between the Ni-200 wick and the Inconel 718 wall appeared to be the reason for the increased Ni concentration in the surface layer.

The depth of the surface layer ranged from 5 to 25 μm (200 to 1000 μin.) and was directly related to the location of the surface in the heat pipe. The depth of the layer was slightly greater in the condenser section than in the evaporator section of the heat pipe. The variation in reaction layer depths, combined with deposits containing Ni, Nb, Fe, and Cr in the evaporator, indicates that material was transferred from the condenser to the evaporator by the sodium liquid and vapor flow.

1.0 INTRODUCTION

The component test power converter (CTPC) is a limited-life (<10,000 hr), laboratory test engine being developed to demonstrate the feasibility of free-piston, Stirling-cycle engine technology for space power conversion applications. The CTPC is designed to operate on thermal energy provided via a sodium metal heat pipe system operating at temperatures to 1050 K (1430°F) with a condenser heat flux of 25 W/cm^2. The unique heat pipe system design minimizes the number of welded or brazed joints operating at elevated temperatures by integrating the CTPC's heater head directly with the heat pipe. In this configuration, regions of the integrated heater head/heat pipe are exposed to condensing sodium vapor, a mean stress of 145 MPa (21 ksi), and a cyclical stress of ±21 MPa (3 ksi). The heater head and heat pipe will be fabricated from Inconel 718.

The vapor and liquid dynamics in an operating heat pipe system result in liquid metal exposure conditions that are very different from those observed in pumped or flowing-loop systems. Thermal energy input at the heat pipe's evaporator generates pure sodium vapor in the working fluid. The vapor flows to the heat pipe's condenser, where thermal energy is extracted, causing the vapor to condense on the heat pipe wall. The condensed liquid is then pulled back to the evaporator by the capillary action of a wick structure within the heat pipe.

Laboratory testing is planned for the CTPC and heat pipe system to confirm the basic design concept and identify areas for further development. However, prior to full-scale engine testing, additional information is required to confirm the mechanical properties and corrosion resistance of nickel-based superalloys in liquid sodium heat pipe systems. The limited data that are available on nickel-based alloys in liquid sodium were primarily generated in flowing-loop systems for nuclear reactor applications and are not directly applicable to the heat pipe environment.

Therefore, to obtain more specific data, a heat pipe fatigue test specimen (HPFTS) was constructed and tested. The HPFTS was subjected to creep and fatigue loads during elevated-temperature operation to evaluate the corrosion resistance and mechanical performance of a sodium-filled Inconel 718 heat pipe. The test was designed to simulate the stress, temperature, and sodium exposure conditions in the most highly stressed region of the CTPC heat pipe system during the planned laboratory testing.

This report describes the test procedures used and presents the findings of the metallurgical analysis conducted on the HPFTS after test completion.

2.0 PROCEDURES

2.1 Test Specimen Components

The HPFTS, shown in Figure 1, consisted of a heat pipe envelope, wick, end caps, and attachment fixturing. Inconel 718 was used for the heat pipe envelope and end caps. The wick was fabricated from 200 mesh Ni-200 screen, with a wire diameter of 0.05 mm (0.002 in.). Commercially pure sodium was used as the working fluid. The compositions of the Inconel 718, the Ni-200 screen material, and the sodium are identified in Table 1.

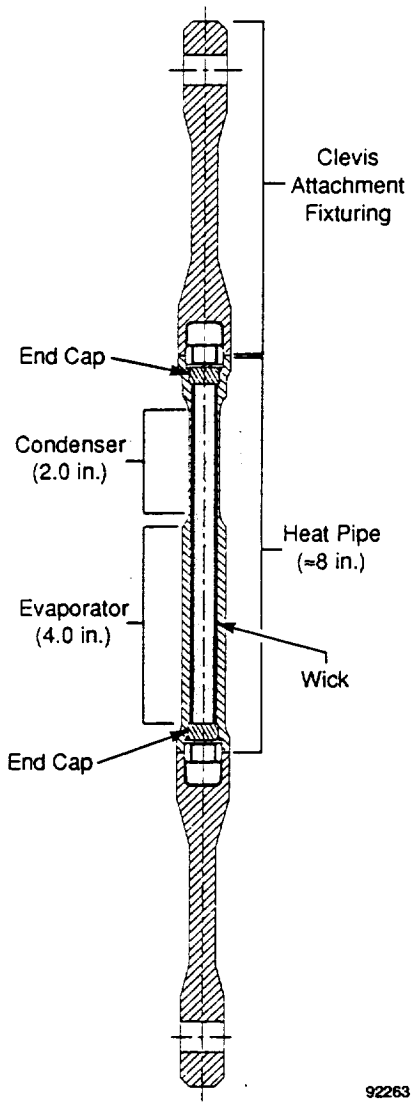

Figure 1. Heat Pipe Fatigue Test Specimen

Table 1. Material Compositions

Element	Inconel 718 (Weight %)	Ni-200 (Weight %)	High-Purity Sodium* (ppm)
Ag	–	–	<3
Al	0.56	–	13
B	–	–	<13
Ba	–	–	<25
Be	–	–	<3
C	0.04	0.03	–
Ca	–	–	13
Cd	–	–	<25
Co	–	–	<13
Cr	18.45	–	<13
Cu	–	–	10
Fe	19.03	0.07	20
K	–	–	625
Li	–	–	<3
Mg	–	–	8
Mn	0.07	0.14	3
Mo	3.07	–	<25
Na	–	–	Balance
Nb	5.18	–	–
Ni	52.10	99.65	<13
Pb	–	–	<13
Rb	–	–	<25
Si	0.12	0.04	13
Sn	–	–	<13
Ti	0.98	0.01	<25
V	–	–	<13
Y	–	–	<25
Zn	–	–	<125
Zr	–	–	<25

*Oxygen concentration of the sodium was not available.

91TR56

The heat pipe envelope was fabricated from 32 mm (1-1/4 in.) diameter Inconel 718 bar stock, AMS 5662, and was approximately 203 mm (8.0 in.) in length with an internal diameter of 12.7 mm (0.5 in.). The pipe condenser was 51 mm (2 in.) long, with a wall thickness of 1.6 mm (0.062 in.). The evaporator was 102 mm (4 in.) long, with wall thickness of 4.8 mm (0.19 in.). The difference in wall thickness ensured that the most severe stress conditions were obtained in the condenser to best simulate the conditions that would be experienced during CTPC laboratory testing. The highest stress in the CTPC heat pipe system under development occurs at the outer edge of the heater head fins, as shown in Figure 2.

The CTPC heat pipe condenser will be fabricated using a combination of conventional milling, electro-discharge machining (EDM), and chemical milling. Chemical milling will be used to remove the recast layer generated by the EDM process. To simulate the surface condition expected in the highest-stress region, the internal bore of the HPFTS was finished by chemical milling. The surface finish after chemical milling was measured at 1.5 μm (60 μin.). A typical chemically milled surface is shown in Figure 3.

2.2 Test Specimen Assembly

The HPFTS components (heat pipe envelope, wick screen, end caps) were degreased in trichloroethane, a water-based detergent cleaning solution, and rinsed in deionized water. To assemble the wick, two layers of the Ni-200 screen were wrapped on a preoxidized stainless steel mandrel, inserted into the heat pipe envelope, and sintered at 1273 K (1832°F) for 30 min. The pipe was cooled to room temperature, the mandrel removed, and the screen spot welded to the heat pipe wall.

A 51 mm (2.0 in.) long, 99.5%-pure vanadium wire was inserted into the heat pipe for use in determining the oxygen content of the sodium working fluid after testing. The procedure to be used was a variation of the V-wire equilibration technique described in ASTM test method C997-83, sections 65 to 74. However, review of the testing requirements after HPFTS fabrication and assembly revealed that this technique was not viable for determining oxygen in the HPFTS due to the method's low detection limits (<15 ppm) [1, 2]*. The V-wire was left in the heat pipe but was not used for analysis.

The heat pipe envelope was sealed with Inconel 718 end caps, which were tungsten inert gas (TIG) welded to the ends of the pipe. A 6.4 mm (0.25 in.) outside diameter Inconel 718 tube, with a 1.6-mm (0.063 in.) wall, was placed in one of the end caps to allow for sodium filling.

The heat pipe was charged with 10 grams of sodium metal using a push pot assembly and sealed with a high-temperature sodium service valve in an argon gas purged dry box. The pipe was heated at 928 K (1211°F) for 1-3/4 hr and 1123 K (1562°F) for 5 min in a vacuum of approximately 2.7×10^{-3} Pa to remove noncondensible gas and optimize the sodium fluid charge. The fill tube was then sealed by electric resistance welding in the vacuum chamber and operated in vacuum at 1123 K (1562°F) for approximately 10 min to ensure complete sealing of the fill tube.

Attachment fixturing was electron beam welded to the ends of the heat pipe. The entire HPFTS was vacuum heat treated according to the following schedule:

- 1227 K (1750°F) 1 hr argon gas cool
- 991 K (1325°F) 8 hr cool to 894 K (1150°F) at 55 K/hr (100°F/hr)
- 894 K (1150°F) 8 hr furnace cool to room temperature.

*Numbers in brackets indicate references listed in Section 6.0.

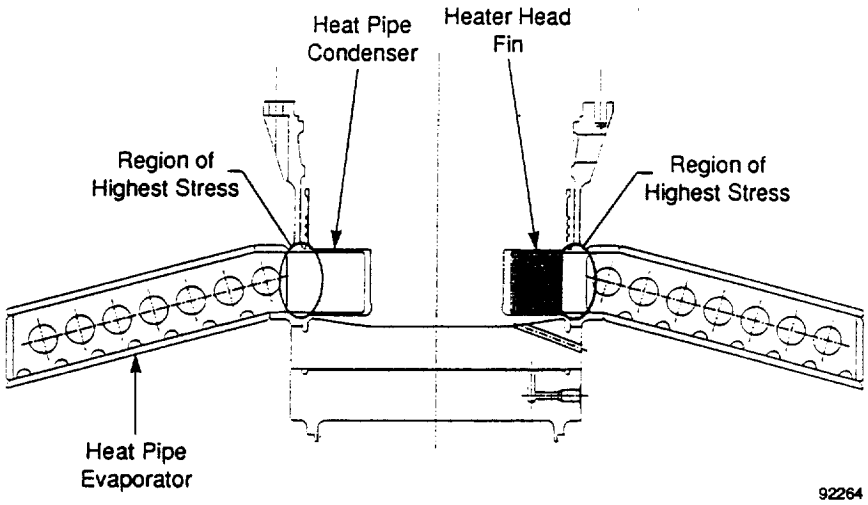

Figure 2. Component Test Power Converter (CTPC) Heater Head and Heat Pipe System Cross Section

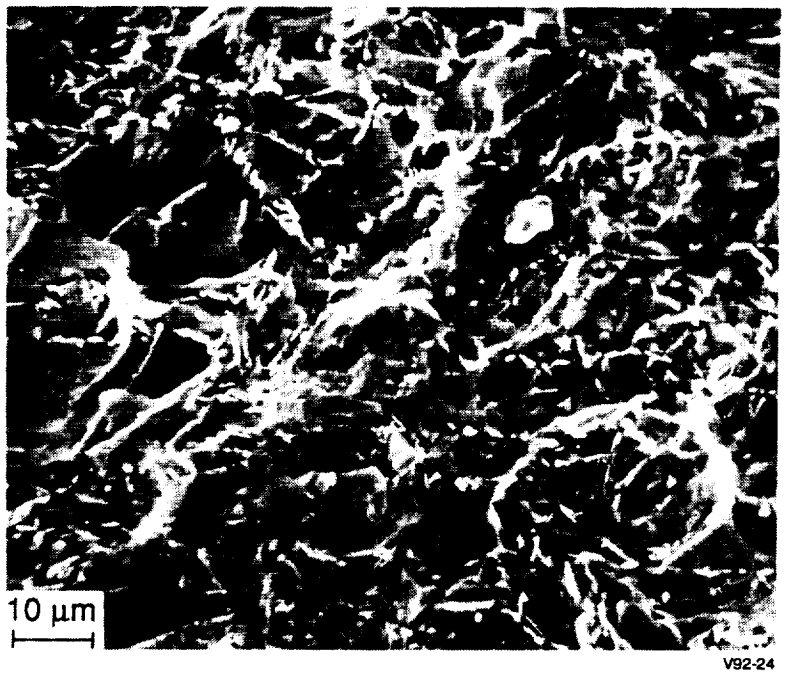

Figure 3. Scanning Electron Micrograph of an Inconel 718 Surface After Chemical Milling

2.3 Test Setup and Conditions

Under actual operating conditions, the highest-stress region of the CTPC heat pipe (Figure 2) will be exposed to condensing sodium vapor, elevated temperature, and combined static and cyclic mechanical loads. The sodium exposure, temperature, and stress conditions for the HPFTS were designed to simulate this region.

The HPFTS was enclosed in a stainless steel chamber (see Figure 4). The chamber was continuously purged with argon during testing to minimize external oxidation and the hazard of a sodium fire if heat pipe failure occurred. The HPFTS was tested in a vertical orientation, with the condenser above the evaporator, which allowed gravity to assist fluid transfer to the evaporator. The evaporator was heated by radiation from two 360-W, 60.3 mm (2.38 in.) inner diameter, half shell electric resistance heaters. The condenser cooled passively by conduction to the ends of the HPFTS and by radiation to the stainless steel enclosure. The estimated heat flux at the condenser was <5 W/cm^2.

The HPFTS was subjected to 36 test sequences under thermal and mechanical load for a total test time of 1090 hr. Maximum temperatures in the condenser were 1000 K (1340°F) or 1050 K (1430°F), depending on the test sequence being conducted. Total hours at specific condenser temperatures were: 775 hr at 950 K (1250°F), 275 hr at 1000 K (1340°F), and 40 hr at 1050 K (1430°F). These operating times and temperatures were shown to produce approximately 2% creep in independent creep tests. Creep strain was not recorded during heat pipe testing. Temperature was monitored with type K thermocouples at ten locations along the length of the heat pipe. A plot (Figure 5) of the

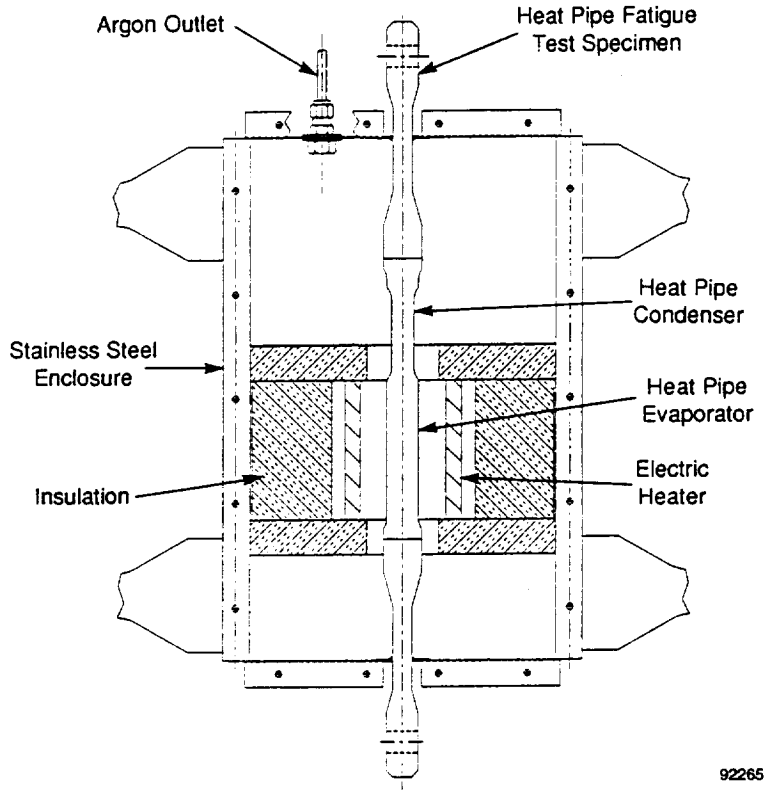

Figure 4. Heat Pipe Fatigue Test Setup

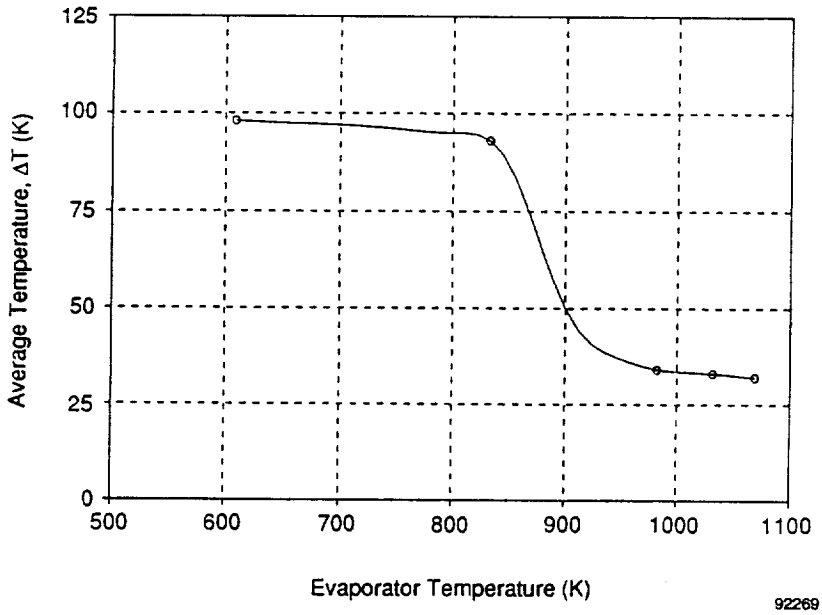

Figure 5. Difference in Average Outside Wall Temperature Between Evaporator and Condenser as a Function of Average Evaporator Temperature

difference in average outside wall temperature between the evaporator and condenser, ΔT, as a function of the average outside wall temperature of the evaporator shows a significant drop in ΔT at evaporator temperatures above approximately 900 K (1160°F). The internal temperature drop along the length of the heat pipe was estimated to be approximately 70 K (125°F) at temperatures below 900 K (1160°F), and <5 K (10°F) at temperatures above 925 K (1205°F).

The mechanical load remained the same for all sequences: 145 MPa (21 ksi) mean stress and ±35 MPa (5 ksi) cyclic stress. During a test sequence, the load cycle was controlled using load response feedback. A typical test sequence, shown in Figure 6, consisted of the following steps:

1. A 145 MPa (21 ksi) mean stress was applied to the heat pipe condenser at room temperature to simulate initial CTPC pressurization with He at 150 bar.
2. Heat was applied to the evaporator until the condenser temperature reached 950 K (1250°F), simulating heat pipe system start-up.
3. A cyclic stress of ±35 MPa (5 ksi) at 70 Hz was applied in addition to the mean stress to simulate the pressure wave in the operating CTPC with an added 14 MPa (2 ksi) safety factor.
4. Depending on the sequence being conducted, the condenser temperature was increased to either 1000 K (1340°F) or 1050 K (1430°F) after 10 to 20 hr of operation at 950 K (1250°F).
5. The HPFTS continued to operate to the end of the test sequence under load at the higher temperature to simulate CTPC operation at higher temperatures.
6. At the end of the test sequence, the cyclic stress was removed and the heater turned off to allow the heat pipe to cool.
7. When the external heat pipe wall at the evaporator reached a temperature of 421 K (300°F), the mean stress was removed to simulate CTPC shutdown.
8. Testing was resumed immediately with the next test sequence.

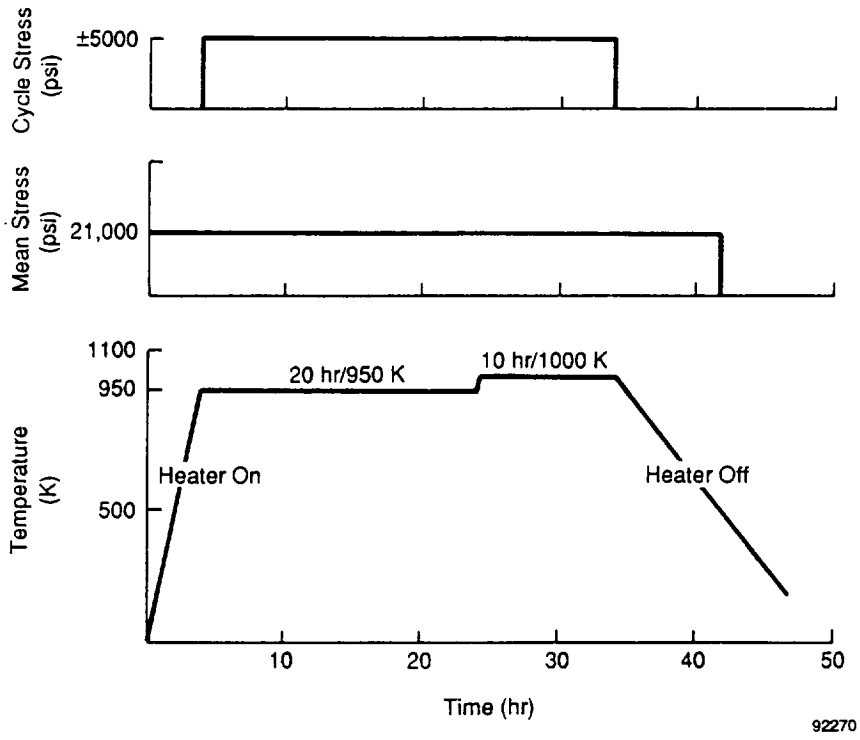

Figure 6. Typical Test Sequence

2.4 Test Specimen Preparation for Analysis

After completion of the 1090-hr fatigue test, the HPFTS was prepared for metallurgical analysis. The attachment fixtures were cut from the ends of the heat pipe. The heat pipe was cut across its diameter in the condenser using a slow-speed diamond saw with a mineral oil lubricant under an argon gas purge.

Sodium was removed from the heat pipe sections by immersion in alcohol. The two heat pipe pieces were submerged in a 50/50 mixture of butyl and propyl alcohols, and the sodium was allowed to react with this mixture for several hours. The pipe was then transferred to a mixture of methyl and ethyl alcohols to continue the reaction process. The total time the pieces were submerged in the alcohols was approximately 24 hr. Final sodium removal was performed in methyl alcohol with intermittent vibration in an ultrasonic cleaner for approximately 12 hr.

Longitudinal cuts were made along two lines approximately 180° apart using an abrasive cut-off wheel and water lubrication. The abrasive wheel cuts were made only through the depth of the heat pipe wall to avoid damaging the wick. The wick was then carefully sectioned along the same two cut lines using surgical scissors and a scalpel. The resulting four pieces were then submerged in ethyl alcohol and vibrated in an ultrasonic cleaner.

2.5 Specimen Analysis

Metallographic sections of the wick and heat pipe wall were prepared from the evaporator and condenser. A JEOL T-300 scanning electron microscope equipped with a Tracor Northern TN-200 energy dispersive x-ray analysis system was used to examine the wick and wall surfaces. Electron microprobe analysis using a JEOL 733 Superprobe equipped with a complete wavelength dispersive x-ray spectral (WDS) analysis system was used for quantitative chemical analysis of the metallographic sections.

3.0 RESULTS

The wick and heat pipe appeared to be in very good condition after sectioning and cleaning, showing no visible signs of corrosion attack. The only visually noticeable effect of sodium exposure was a metallic-looking deposit on the wick over a 25.4 mm (1.0-in.) length at the base of the evaporator (see Figure 7*). The metallographic analysis, however, did produce evidence of localized corrosion.

3.1 Wick

Scanning electron microscope examination of the metallic-looking deposit at higher magnification revealed that the wick was fully coated by the deposited material, as shown in Figure 8. The diameter of the wire in the specimen increased from 0.050 mm (0.002 in.) to approximately 0.076 mm (0.003 in.).

Many of the wires with the heaviest deposits were observed to have a central core surrounded by an outer shell, as can be seen in Figure 9. The compositions of the outer shell and central core were examined using WDS analysis on polished metallographic sections. The outer shell contained approximately 80% Ni and 20% V with the concentration of V gradually decreasing toward the central core. The central core was nearly pure Ni with <1% V. A slight increase in Cr and O was also observed at the outer edge of the wire deposit. Table 2 lists the concentration of elements in the deposited material from three locations on the wire cross section.

The wick wires were not significantly changed in regions away from the base of the evaporator. No measurable change in wire diameter was observed in the upper regions of the evaporator or in the condenser. Grain boundary etching was the only noticeable effect of sodium exposure in these regions (see Figure 10). No change in wire chemistry was detected with WDS analysis.

A second type of deposit was observed in a small area approximately 44.5 mm (1.75 in.) above the base of the evaporator. The location of the deposit is suspected of corresponding with the region of contact between the V-wire and the heat pipe wall but this could not be confirmed. In this region, a cluster of crystals containing Ni and V with small additions of Nb, Cr, Al, Ca, Si, C, and O was formed on the wick as shown in Figure 11. WDS analysis on the as-deposited material was used to estimate the concentration of these elements in the deposit. The analysis results are given in Table 3. The Ca, Si, C, and O appeared to be concentrated in nodules attached to the crystal surface as shown in Figure 12.

3.2 Heat Pipe Wall

Scanning electron microscopy was used to examine the heat pipe wall for evidence of surface corrosion. Fine surface pits, <1.5 μm (60 μin.) in diameter, were observed at the evaporator base to a height of approximately 25.4 mm (1.0 in.) (see Figure 13). The pitted region corresponded with the region of the wick that was coated with the vanadium-containing deposits. Exposure to excess sodium liquid accumulated at the base of the evaporator appears to be the reason for the surface changes observed in this region. The maximum depth of the fine surface pits was <10 μm (400 μin.) as revealed by metallographic sections (Figure 14). The intensity of pitting gradually decreased at distances greater than 25.4 mm (1.0 in.) from the evaporator base and no fine surface pits were observed above approximately 51 mm (2 in.) (Figure 15).

The condenser wall was faceted as a result of surface etching, with the most significant etching occurring in the lower 32 mm (1.25 in.) of the condenser (Figure 16). The faceted surface was not observed above approximately 38 mm (1.5 in.) into the condenser (Figure 17). Limited vapor flow

---

*Due to the large number of figures and tables in this section, they are included at the end of the text in their order of reference.

resulting from a build-up of noncondensible gas or excess sodium metal are probable explanations for the lack of etching at the condenser end.

A surface layer, appearing white in etched metallographic sections, was observed on all heat pipe surfaces exposed to sodium during testing (Figure 18). The layer is thought to result from a change in base metal surface chemistry due to interaction with the high-temperature sodium metal. The thickness of the layer was approximately 15 to 25 μm (600 to 1000 μin.) in the evaporator and 5 to 10 μm (200 to 400 μin.) in the condenser.

WDS analysis results, presented in Table 4, indicated that the concentrations of Cr, Nb, Al, and Ti were reduced and the concentration of Ni was increased in the layer relative to the nominal alloy composition. The concentrations of Fe and Mo were reduced slightly in some locations. An average layer composition, calculated from data taken at several locations in the evaporator and condenser, indicated that the changes in Cr, Fe, Ni, and Mo concentration were more pronounced in the condenser. All composition data used in the average calculation were taken at 2 to 3 μm (80 to 120 μin.) below the sodium-exposed surface.

Knoop microhardness measurements were taken in the surface layer and the unaffected heat pipe material. The surface layer hardness was approximately 203 KHN and the unaffected Inconel 718 was 435 KHN, indicating a significant reduction in surface hardness.

In addition to the surface changes discussed above, the concentration of grain boundary carbides was reduced at the sodium-exposed surface (Figure 19). The grain boundary carbides were affected to a depth of 25 to 30 μm (1000 to 1200 μin.). Depletion of carbides was observed in both the evaporator and condenser. Metallographic sections revealed that some carbides exposed to the sodium were being dissolved and leached from the surface (Figure 20).

A small region of more extensive corrosion was observed approximately 44.5 mm (1.75 in.) above the base of the evaporator. The depth of attack in this region was approximately 35 μm (1400 μin.), as shown in Figure 21. The reason for accelerated corrosion at this location is not certain but is suspected of corresponding with the contact area between the V-wire and the heat pipe wall. Accumulation of liquid sodium with a high concentration of oxygen contamination is thought to be the reason for the local corrosion mechanism. Table 5 provides the results of the WDS analysis of the corrosion product and white regions in the base metal adjacent to the corrosion product.

The corrosion product remained in the surface pits after sectioning and cleaning with alcohol and water. WDS analysis showed that the chemical composition of the corrosion product was similar to sodium-chromium-oxygen compounds observed in 300 series stainless steels exposed to high-oxygen sodium [3]. Fe, Ni, Nb, Al, and Ti were also observed in the corrosion product formed in Inconel 718.

As indicated in Table 5, the white regions in the base metal adjacent to the corrosion product were depleted in Cr, Nb, Al, and Ti and enriched in Ni. The concentration of Fe and Mo, 18.8% and 3.9% respectively, showed little change from the nominal alloy concentration of 19.0% Fe and 3.1% Mo.

Crevices at the ends of the pipe were examined for signs of accelerated corrosion. The locations of these crevices is shown in Figure 22. Minor grain boundary attack, <10-μm (400 μin.) deep, was observed in metallographic sections from the evaporator crevices (see Figure 23). A larger, local pit was observed in a metallographic section from the condenser, Figure 24. Several metallographic sections taken from adjacent regions contained no indications of pitting. The cause of the pit in the condenser crevice could not be identified conclusively. Accelerated corrosion from contamination accumulated in the crevice or a simple defect in the end cap weld are two possible explanations.

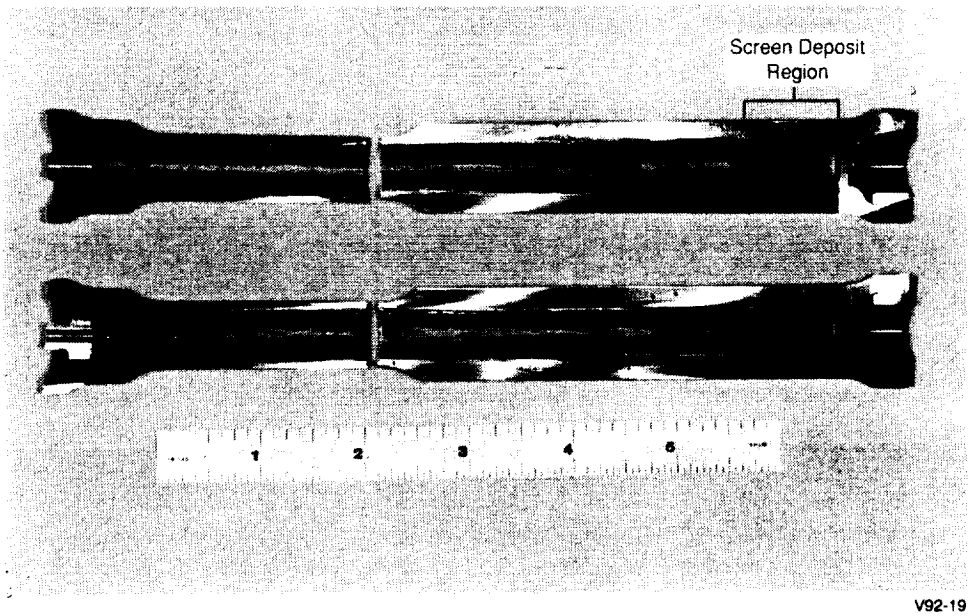

Figure 7. Heat Pipe Fatigue Test Specimen After Sectioning and Alcohol Cleaning

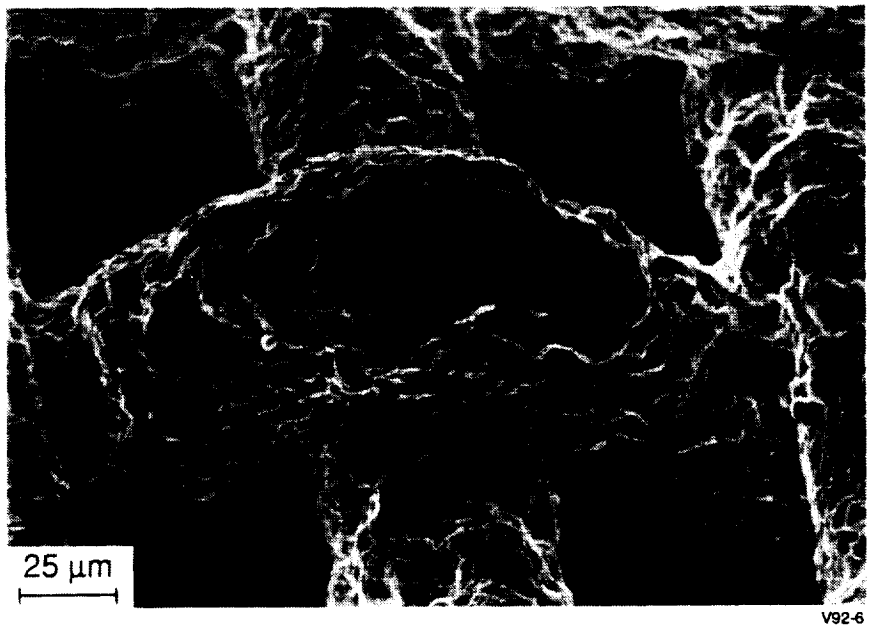

Figure 8. Scanning Electron Micrograph of Wick at Evaporator Base

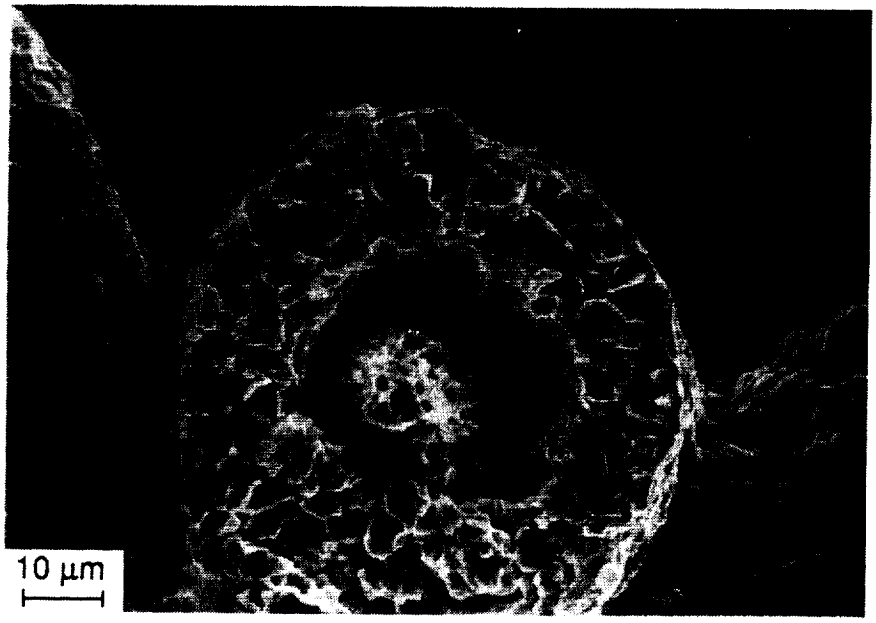

Figure 9. Scanning Electron Micrograph of Fractured Wire in Deposit Region Showing Cored Structure

Table 2. Nominal and Post-Test Compositions of Wick from Lower Evaporator

Element	Nominal Ni-200 (Weight %)	Post-Test from Three Wire Locations		
		Outer Edge (Weight %)	Mid-Radius (Weight %)	Central Core (Weight %)
Al	–	*	*	*
C	0.03	*	*	*
Cr	–	0.62	0.12	0.14
Fe	0.07	0.12	0.28	0.23
Mn	0.14	0.19	0.35	0.44
Mo	–	*	*	*
Nb	–	*	*	*
Ni	99.65	76.80	92.50	97.70
O	–	1.60	0.98	0.78
Si	0.04	–	–	–
Ti	0.01	0.14	0.17	0.16
V	–	20.55	5.61	0.54

91TR56

*Concentration below detectable limit.

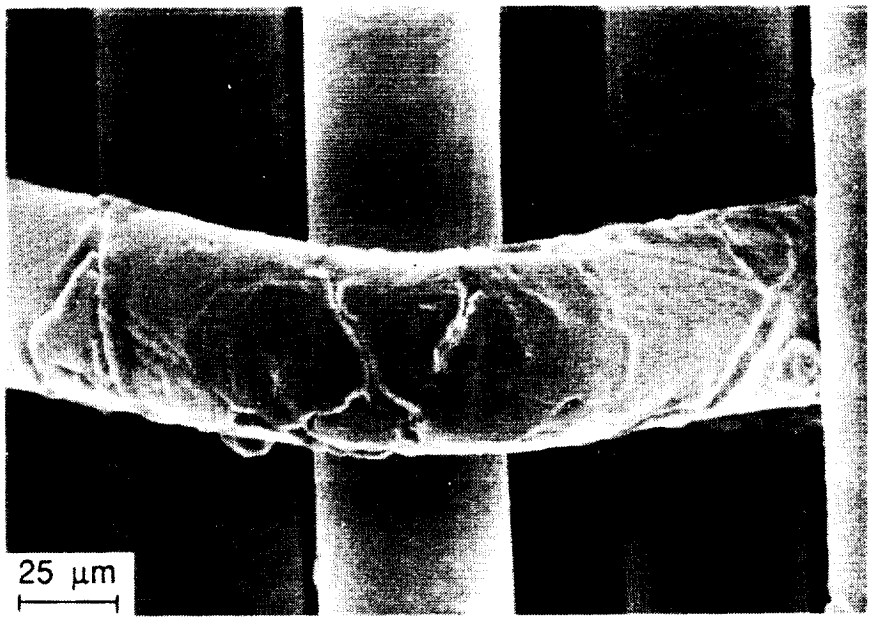

a) Condenser

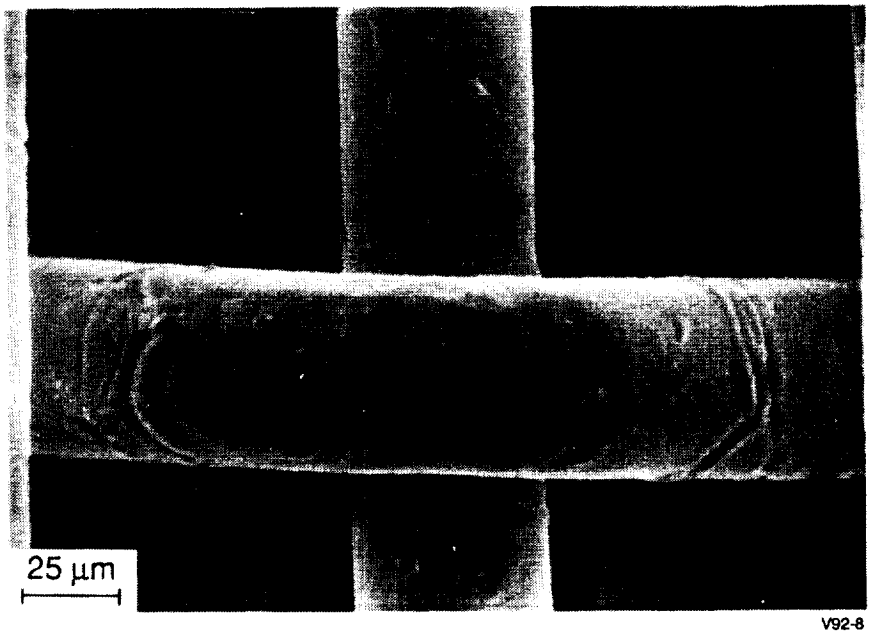

b) Upper Evaporator

Figure 10. Scanning Electron Micrograph of Wick

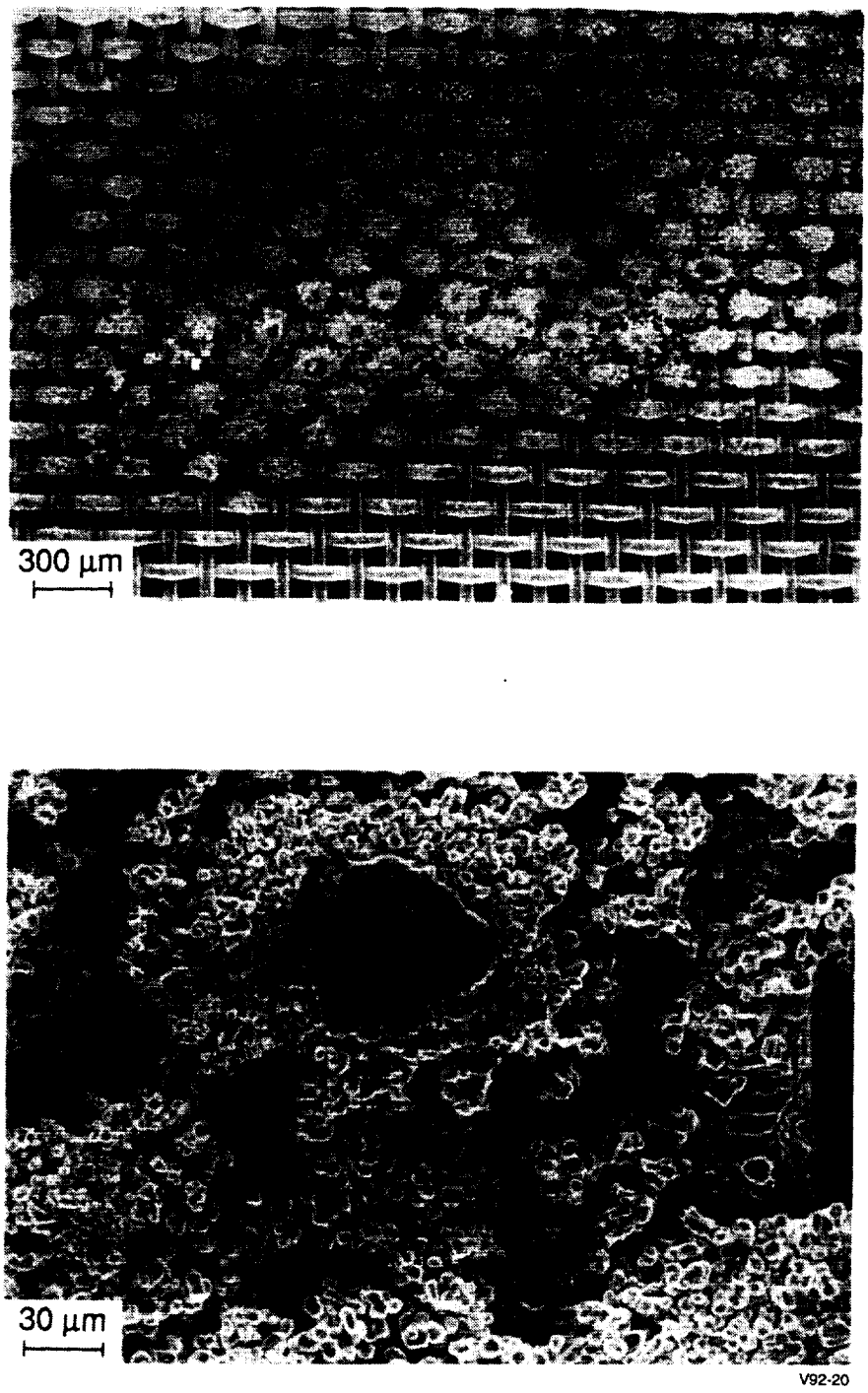

Figure 11. Scanning Electron Micrograph of Screen Deposits in Evaporator

Table 3. Composition of Crystalline Deposit from Lower Evaporator

Element	Deposit Concentration (Weight %)
Al	0.30
C	0.30
Ca	0.51
Cr	0.47
Fe	0.04
Mn	*
Mo	*
Nb	0.87
Ni	72.26
O	3.90
Si	0.07
Ti	*
V	21.27

*Concentration below detectable limit.

91TR56

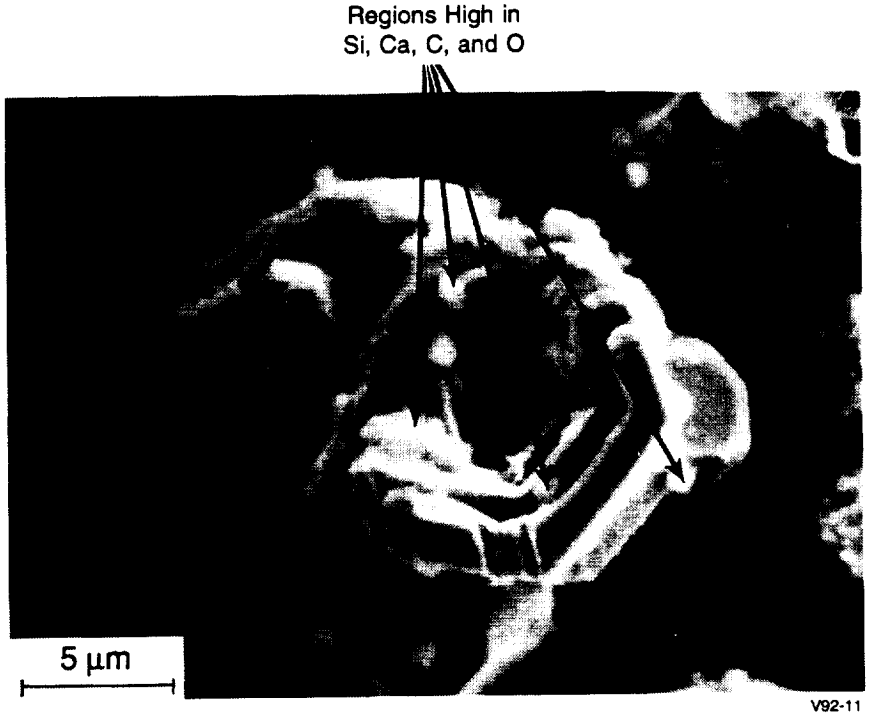

Figure 12. Secondary Electron Image of Screen Deposit in Evaporator

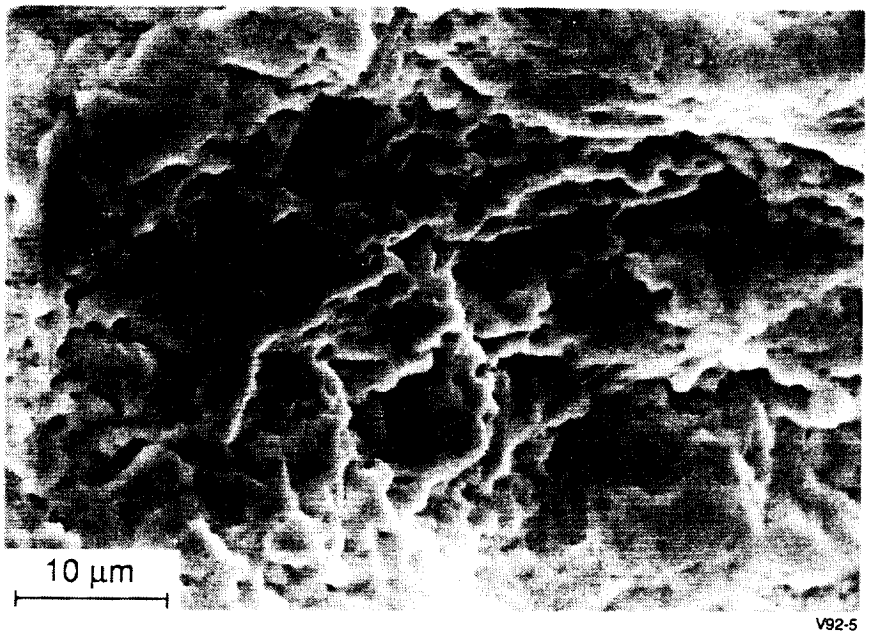

Figure 13. Scanning Electron Micrograph of Inconel 718 Heat Pipe Wall at Evaporator Base

Figure 14. Optical Micrograph of Fine Surface Pitting on Heat Pipe Wall at Evaporator Base

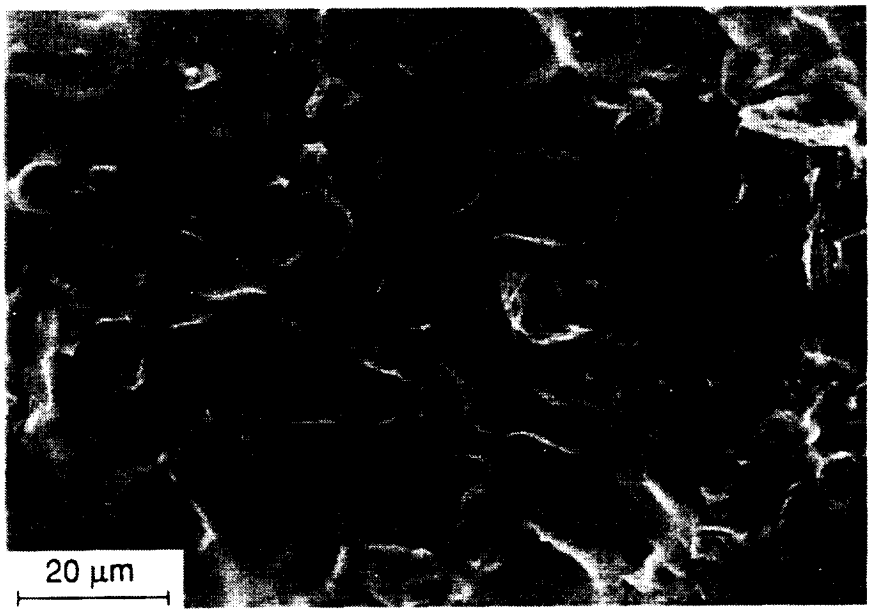

a) 2.0 In. Above Base

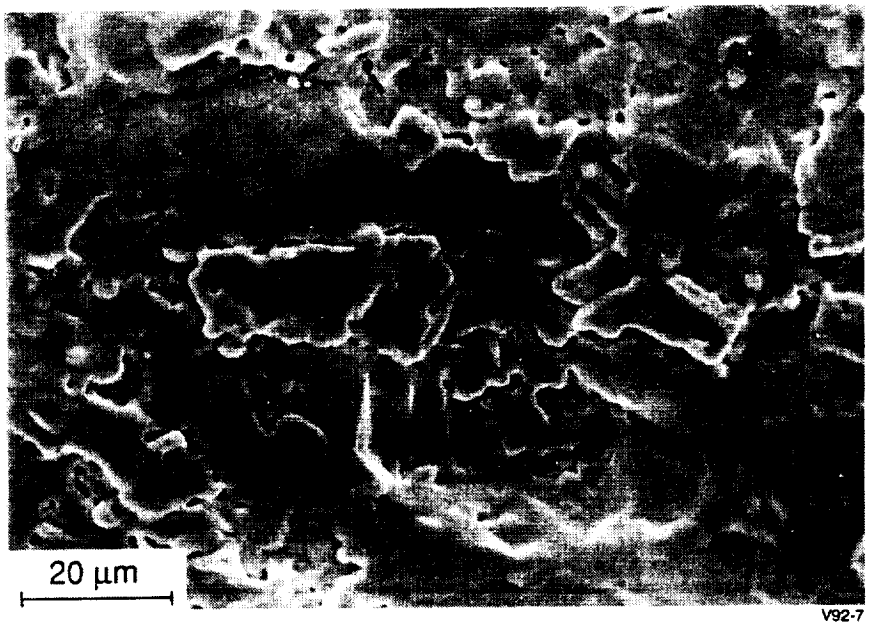

b) 1.25 In. Above Base

Figure 15. Scanning Electron Micrographs of Heat Pipe Wall at Two Locations Above Evaporator Base

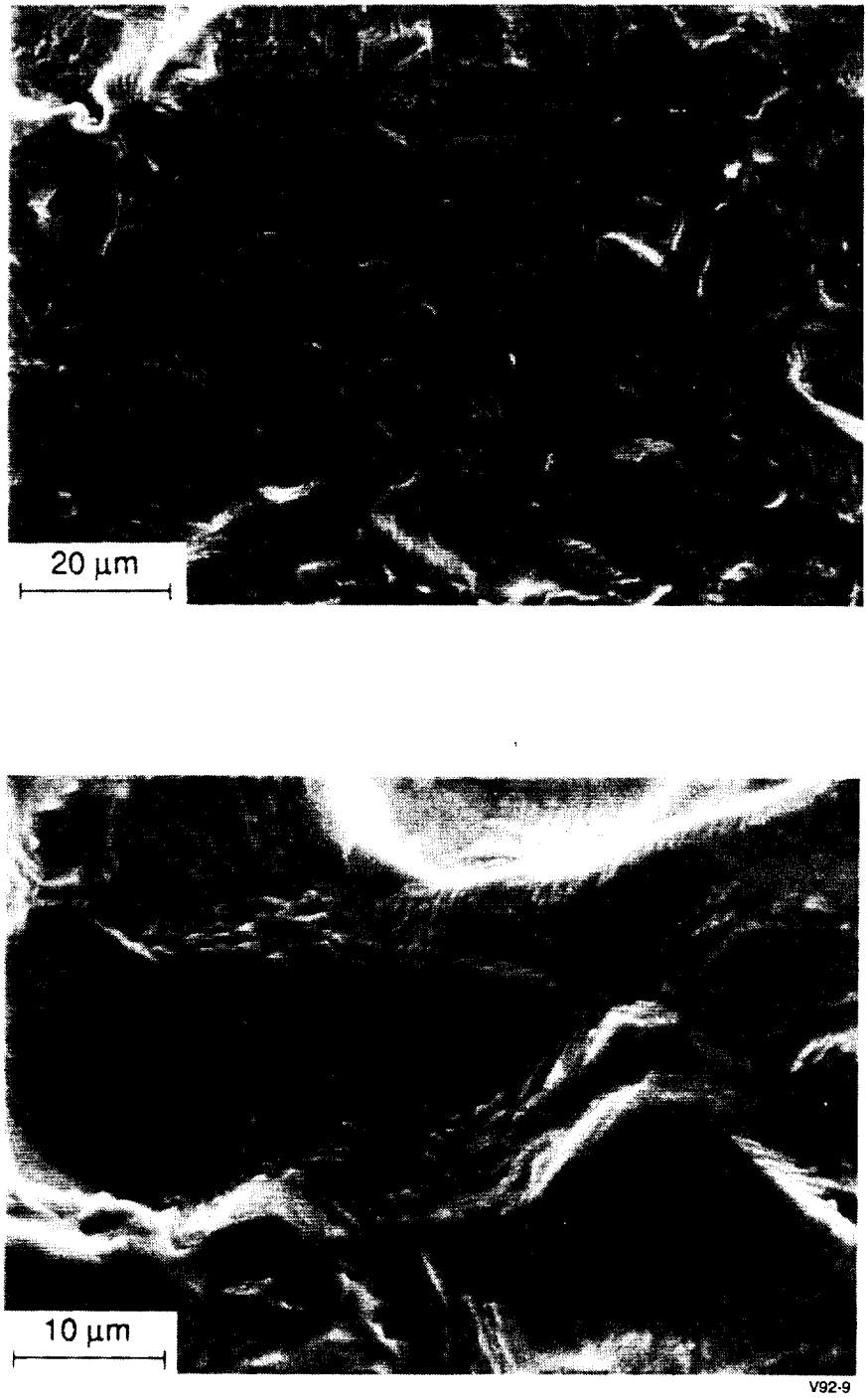

Figure 16. Scanning Electron Micrographs of Faceted Surface in Condenser

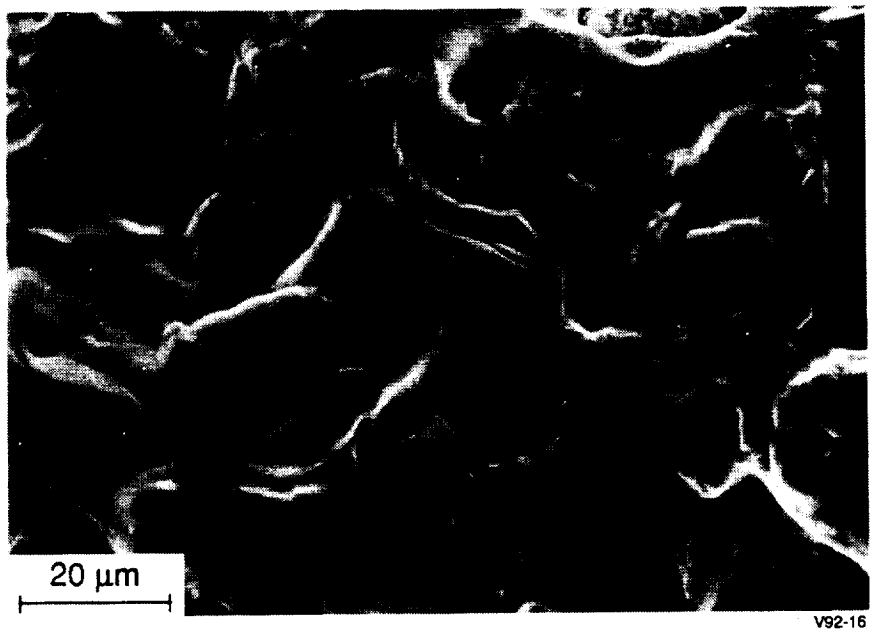

Figure 17. Scanning Electron Micrograph of Heat Pipe Wall Surface in Upper Half of Condenser

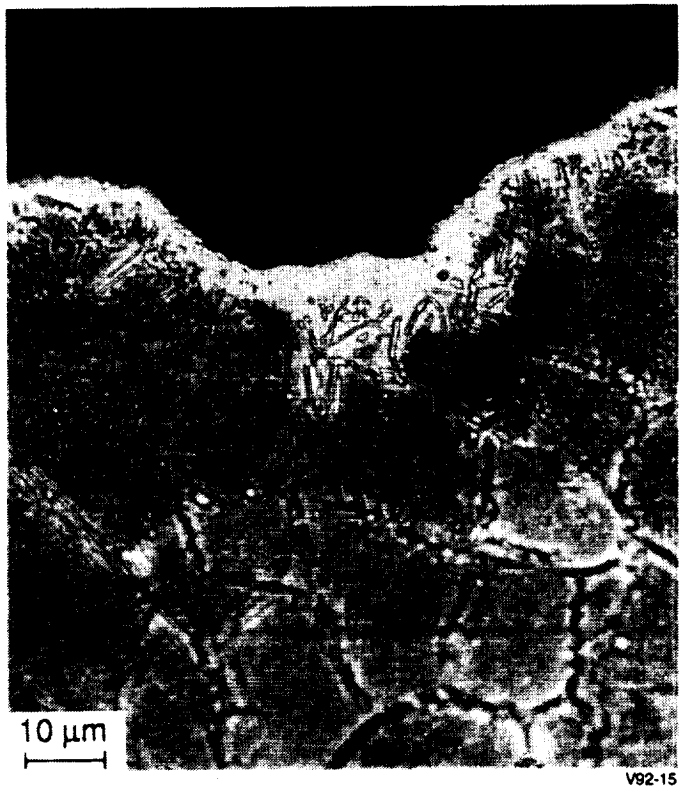

Figure 18. Optical Micrograph of Inconel 718 Surface Layer (White) in Condenser

Table 4. Comparison of Heat Pipe Wall Surface Layer and Nominal Alloy Compositions

Element	Nominal Inconel 718 (Weight %)	Evaporator Surface* (Weight %)	Condenser Surface* (Weight %)
Al	0.56	0.05	0.25
C	0.04	0.00	0.00
Cr	18.45	15.49	11.61
Fe	19.03	18.48	13.76
Mn	0.07	0.05	0.04
Mo	3.07	3.03	2.38
Nb	5.18	1.68	2.23
Ni	52.10	60.10	69.19
O	–	0.08	0.01
Si	0.12	0.00	0.01
Ti	0.98	0.22	0.44
V	–	0.82	0.11

*Average values calculated from WDS analysis, 2 to 3 μm below sodium-exposed surface.

91TR56

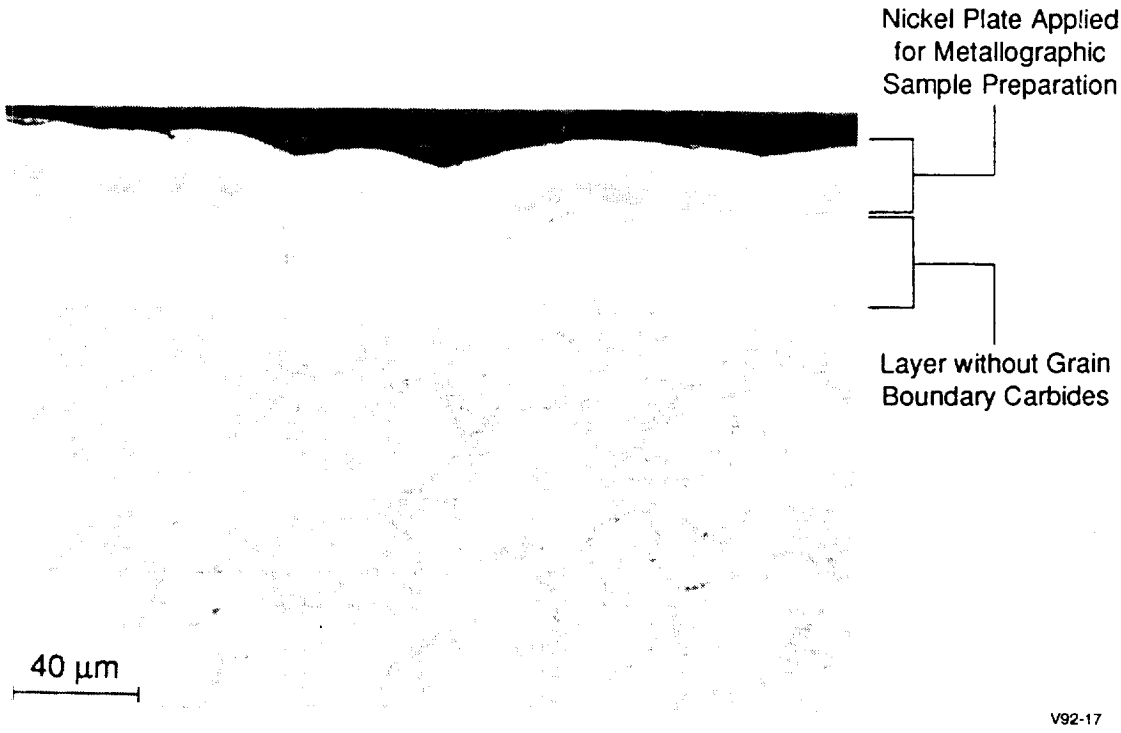

Figure 19. Optical Micrograph of Inconel 718 Surface Layer in Evaporator

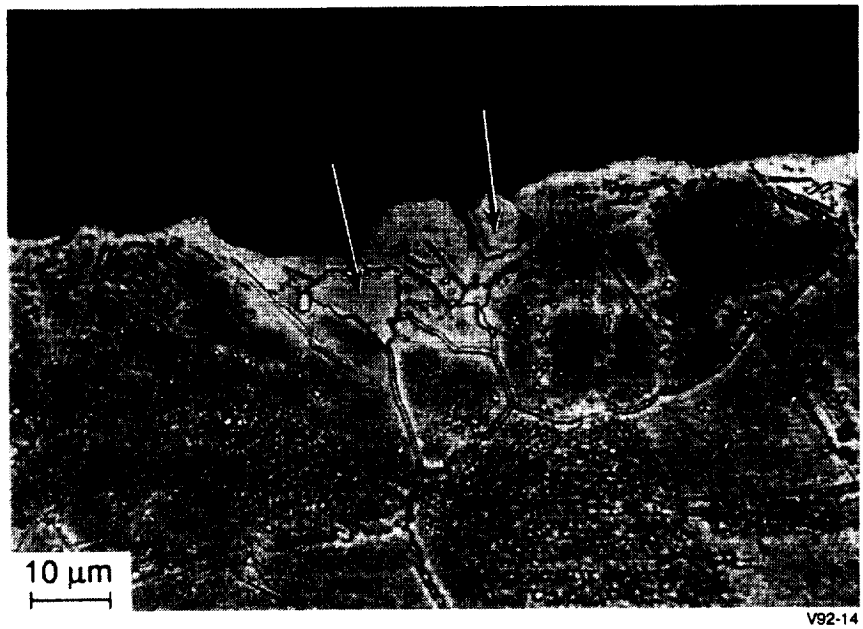

Figure 20. Optical Micrograph of Inconel 718 Carbides Partially Dissolved at Sodium-Exposed Surface (Arrows)

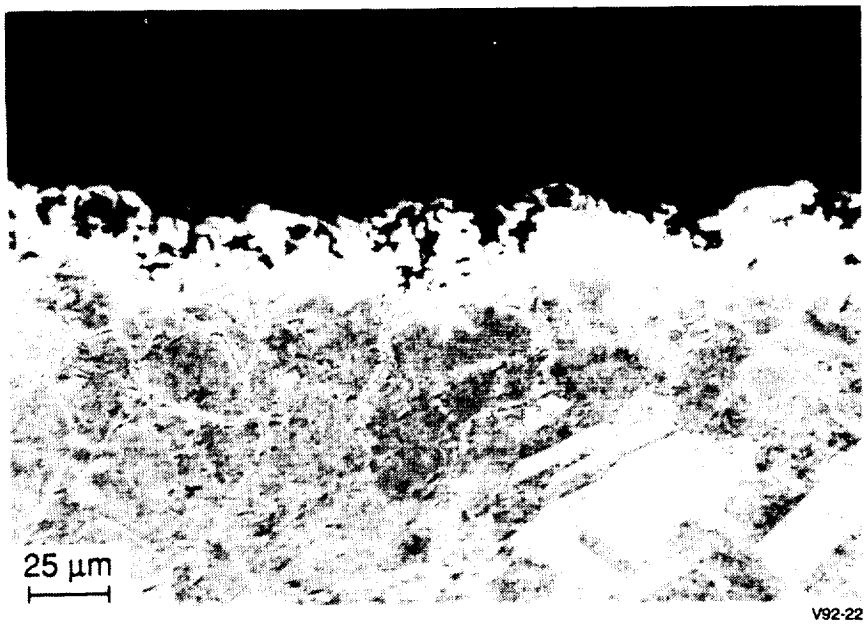

Figure 21. Optical Micrograph of Oxygen-Accelerated Corrosion

Table 5. Comparison of Corrosion Product and White Region with Nominal Alloy Composition

Element	Nominal Inconel 718 (Weight %)	Corrosion Product (Weight %)	White Region (Weight %)
Al	0.56	0.39	0.05
C	0.04	0.00	0.00
Cr	18.45	49.50	7.91
Fe	19.03	1.03	18.80
Mn	0.07	0.00	0.06
Mo	3.07	0.77	3.94
Na	–	1.64	0.00
Nb	5.18	3.09	0.39
Ni	52.10	3.22	68.73
O	–	39.69	0.00
Si	0.12	0.00	0.00
Ti	0.98	0.60	0.08
V	–	0.06	0.04

91TR56

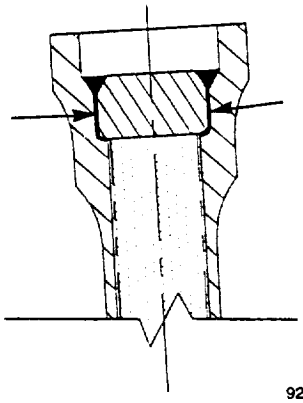

Figure 22. Heat Pipe End Cap Crevices (Arrows)

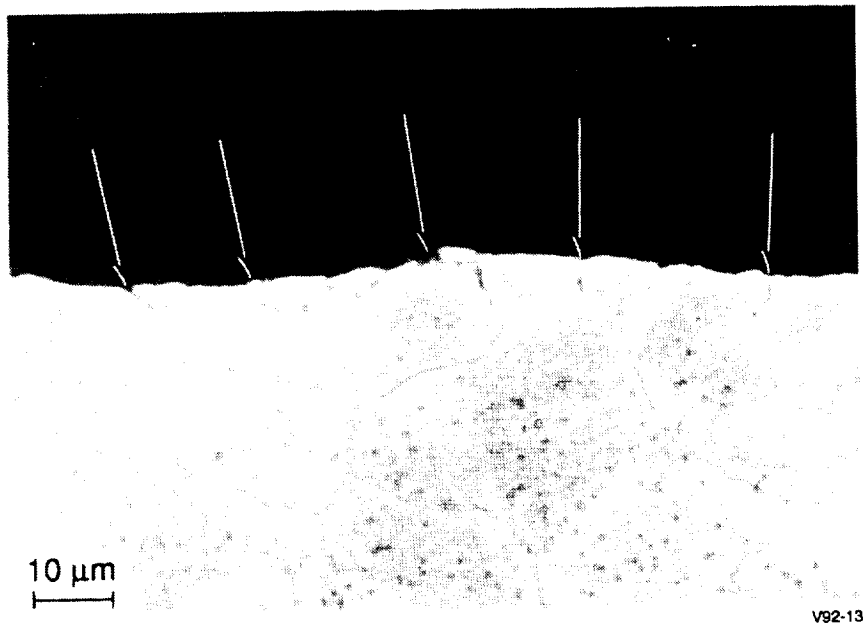

Figure 23. Optical Micrograph of Exposed Inconel 718 in Evaporator End Cap Crevice with Limited Grain Boundary Attack (Arrows)

Figure 24. Optical Micrograph of a Pit in Condenser End Cap Crevice

4.0 DISCUSSION OF RESULTS

4.1 Heat Pipe Exposure Conditions

Surface topography changes observed in the Ni-200 wick and the Inconel 718 heat pipe wall indicated that three primary sodium exposure/interaction regions were present along the length of the operating HPFTS. These regions, shown in Figure 25, appear to result from exposure to:

- Condensing sodium vapor and pure sodium liquid (condenser)
- Evaporating sodium and sodium liquid containing moderate levels of contamination and solute (upper evaporator)
- Excess liquid sodium containing a high concentration of contaminants and solute (evaporator base).

4.2 Surface Chemistry

Surface chemistry changes have been observed in 300 series stainless steels and Ni-based alloys exposed to flowing sodium in the hot zone of nonisothermal pumped loops [4, 5]. Surface layers depleted in Cr and Ni and enriched in Fe were formed in the stainless steels. The surface of Inconel 718 exposed to sodium under similar conditions was found to be depleted in Cr, Ni, Nb, and Al and enriched in Fe and Mo.

A surface layer depleted in Cr, Nb, Ti and Al was formed on the Inconel 718 in all regions of the HPFTS. Fe and Mo concentrations were also reduced slightly in the condenser. In contrast to previous observations [4], the Ni concentration at the surface of the Inconel 718 heat pipe increased as a result of sodium exposure. This increase appears to occur because of the large surface area of the Ni-200 wick in proximity to the Inconel 718 and the limited solubility of Ni in sodium, approximately 3.9 ppm at 1050 K (1430°F) [6].

Ni and Ni-based alloys exposed to high-temperature sodium are thought to corrode by dissolution of Ni from the metal surface [7, 8]. The rate of dissolution is directly related to the difference between the concentration of Ni in the sodium and the maximum solubility of Ni in sodium at the test temperature. The rate of Ni loss from the surface can be described by the equation:

$$J = k(C - c)$$

where:

J = rate of Ni dissolution
k = solution rate constant
C = solubility of Ni in sodium at the temperature of interest
c = actual concentration of Ni in the sodium.

The surface area of the Ni-200 wick was estimated to be more than five times the surface area of the Inconel 718 heat pipe wall. Based on the area of surface exposed, the wick has the potential of providing five times more Ni than the wall in a given period of time. In addition, the concentration of Ni is 52% in Inconel 718 and 99.6% in the Ni-200 wick, which again favors dissolution of Ni from the wick. The sodium is thought to be saturated with Ni, supplied primarily by the wick, thus limiting dissolution of Ni from the heat pipe wall.

Limited dissolution of Ni combined with leaching of Cr, Nb, Ti, and Al from the Inconel 718 resulted in a relative increase of Ni at the sodium-exposed surface.

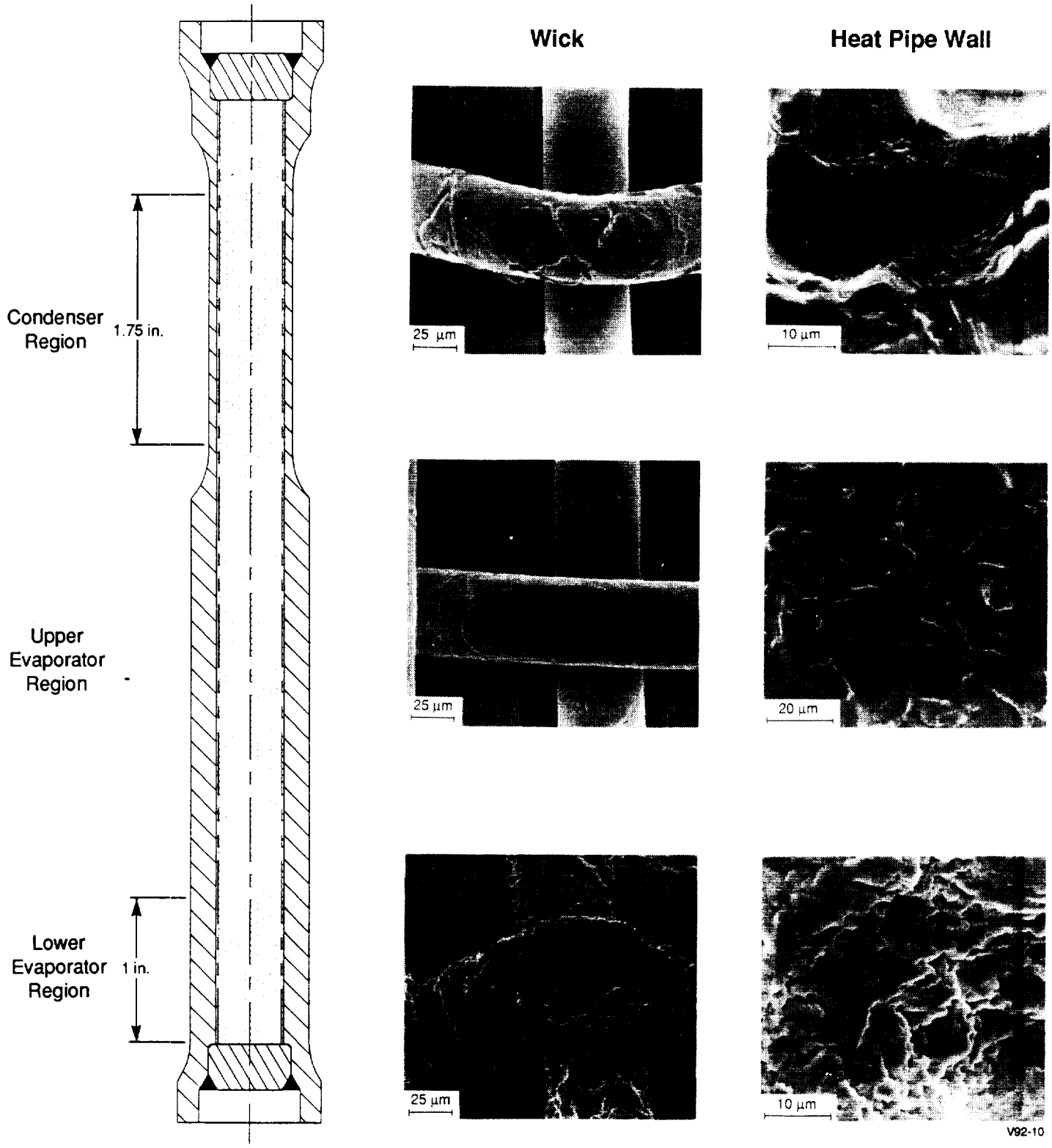

Figure 25. Three Primary Interaction Regions Along Heat Pipe Length

Low microhardness values observed in the white etching surface layer correlate well with reduced concentrations of Nb, Al, and Ti. The high strength of age- hardened Inconel 718 is generated by precipitation of Nb-rich Ni3 (Nb, Ti, Al), also known as γ'' [9]. Low concentrations of Nb, Al, and Ti, as observed in the surface layer, will reduce the amount of γ'' and result in low strength and hardness.

Interaction between the wick and wall materials was found to have a strong influence on surface chemistry changes and dissolution rates in the sodium heat pipe environment. The current CTPC heat pipe design specifies 316L stainless steel, containing approximately 10% Ni, for the wick material. The limited concentration of Ni available in the 316L stainless steel will allow the sodium to remove larger concentrations of Ni from the CTPC heat pipe wall before the Ni solubility limit is reached. As a result, a surface layer depleted in Ni is expected in the Inconel 718 exposed in the CTPC heat pipe.

4.3 Mass Transfer

In an operating heat pipe, pure sodium vapor formed in the evaporator flows to the condenser where heat is extracted. Heat removal causes the vapor to condense as a pure liquid. Based on the dissolution rate equation described in Section 4.2, elements that are soluble in liquid sodium will be removed from the heat pipe condenser wall due to the small concentration of solute in the pure sodium liquid. The liquid returns to the evaporator, transferring the solute accumulated from the heat pipe wall to the liquid sodium collected in the evaporator. Here, the solute concentration increases as pure sodium vapor is again formed. Thus, a net transfer of material from the condenser to the evaporator is expected.

Low heat flux rates and the complex interaction of the Inconel 718/Ni/V system made it difficult to confirm this operating mechanism but several factors supporting this theory were observed in the HPFTS. These observations were as follows:

- Deposits containing Ni, Nb, Fe, and Cr formed in the evaporator, confirming the transport of soluble elements to that area. Vanadium from the pure V-wire, included in the heat pipe for oxygen analysis after testing, was also a major constituent in the evaporator deposits. The vanadium appears to be transferred directly through excess sodium liquid without transport through the vapor phase or migration along the length of the heat pipe.
- Changes in surface chemistry were observed in both the condenser and evaporator but greater changes occurred in the condenser. This observation indicates that the dissolution potential is stronger in the condenser, which supports the theory of condenser-to-evaporator mass transfer.
- The thickness of the white etching surface layer observed in the sodium-exposed Inconel 718 was approximately 15 to 25 μm (600 to 1000 μin.) in the evaporator and 5 to 10 μm (200 to 400 μin.) in the condenser. Removal of material through mass transfer is thought to be the cause for the thinner layer in the condenser. This observation also supports the theory of mass transfer in the heat pipe system.

4.4 Local Accelerated Corrosion

A region of accelerated corrosion attack in the heat pipe evaporator appeared to result from a local increase in oxygen concentration in the sodium. It has been shown that sodium chromite, Na2CrO3, and sodium ferrite, Na2O-Fe2O3, can form in 300 series stainless steels exposed to sodium containing >20 ppm oxygen [3, 10]. The concentrations of Cr and O in the corrosion product in the HPFTS were similar to those of sodium chromite observed previously [3]. The Inconel 718 corrosion product also contained Fe, Nb, Ni, Ti, and Al. Crystallographic analysis was not performed to fully characterize the corrosion products.

The relative increase in Ni and Mo concentration in the white etching zone surrounding the corrosion product indicates that these elements are relatively insensitive to the concentration of oxygen in the sodium. The slight reduction in Fe concentration and the large reduction of Cr, Nb, Al, and Ti concentration in the zone surrounding the corrosion product indicate that these materials are more sensitive to the presence of oxygen.

5.0 CONCLUSIONS AND RECOMMENDATIONS

The conclusions reached from the metallurgical evaluation of the HPFTS are as follows:

- Three primary sodium interaction regions were observed in the HPFTS and are expected to be present in the CTPC heat pipe. These regions will correspond with the lowest point in the evaporator, the upper evaporator, and the condenser. The interaction and corrosion mechanisms operating in the CTPC heat pipe are expected to be the same as those observed in the HPFTS, even with increased heat flux.
- Stress-accelerated corrosion, stress corrosion cracking, extensive grain boundary attack, and liquid metal embrittlement were not observed in any region of the HPFTS and are not expected in the CTPC heat pipe.
- Transfer of Ni, Cr, Nb, Fe, and C from the condenser to the evaporator was observed in the HPFTS and is expected to occur in the CTPC heat pipe. The rate of dissolution and deposit formation, i.e., mass transfer, will be increased relative to the rate in the HPFTS due to the increased sodium flux rate.
- Interaction between the heat pipe wick and wall materials has a major influence on the surface chemistry changes occurring in liquid sodium heat pipes. Changing the wick material, i.e., from Ni-200 to 316 stainless steel, will affect the rate of Ni dissolution and mass transfer from the heat pipe wall.
- Regions of oxygen-accelerated corrosion were present in the HPFTS and are expected to occur in the CTPC heat pipe evaporator. Failure of the CTPC heat pipe resulting from this type of corrosion is not expected due to the limited depth of attack (<35 μm (1400 μin.)), the thick wall structure in the CTPC evaporator (6.3 mm (0.25 in.)), and careful control of initial sodium purity.
- The cause of the large pit, 300 to 400 μm (0.012 to 0.016 in.) in depth, observed in the crevice at the end of the heat pipe condenser was not identified conclusively. Therefore, reasonable efforts should be made to minimize crevices in the CTPC heat pipe.

A better understanding of the processes that occur in a heat pipe system will enable the design of future engines to be enhanced and may provide the opportunity to extend the life of long-life engines. Therefore, additional development studies on alkali-metal/nickel-based superalloy heat pipes are recommended to define the effects of:

- Wick material on heat pipe wall corrosion, surface chemistry, and mass transfer
- Alkali metal flux rate on mass transfer
- Alkali metal heat pipe exposure on the long-term creep rate and fatigue resistance of nickel superalloys.

6.0 REFERENCES

1. Hooper, A. J., and E. A. Trevillion. "Oxygen Analysis of Sodium by Equilibration with Vanadium: An Assessment." Journal of Nuclear Materials 48 (1973):216-222.
2. Smith, D. L. "An Equilibration Method for Measuring Low-Oxygen Activities in Liquid Sodium." Nuclear Technology 11 (1971):115-119.
3. Hiltz, R. H. "The Corrosion of Stainless Steel in Oxygen-Contaminated Sodium at 1200°F and 1400°F." Corrosion by Liquid Metals. Edited by J. E. Draley and J. R. Weeks. Plenum Press, 1970.
4. Whitlow, G. A., et al. "Sodium Corrosion Behavior of Alloys for Fast Reactor Applications." In Proceedings of the TMS-AIME Symposium on Chemical Aspects of Corrosion and Mass Transfer in Liquid Sodium, Detroit, October 19-20, 1971.
5. Berkey, E., and G. A. Whitlow. "Microstructural and Compositional Changes in Sodium-Exposed Stainless Steel by Scanning Electron Microscopy." In Proceedings of the TMS-AIME Symposium on Chemical Aspects of Corrosion and Mass Transfer in Liquid Sodium, Detroit, October 19-20, 1971.
6. Weeks, J . R., and H. S. Isaacs. "Corrosion and Deposition of Steels and Nickel-Based Alloys in Liquid Sodium." In Volume 3 of Advances in Corrosion Science and Technology. Plenum Press, 1973.
7. Tyzack, C. "The Behaviour of Materials in Liquid Sodium." In Proceedings of the Symposium on Advances in Materials. Institution of Chemical Engineers, Northwestern Branch, Manchester, England, 1964.
8. Tortorelli, P. F. "Fundamentals of High-Temperature Corrosion in Liquid Metals." In Volume 13 of Metals Handbook, 9th ed. American Society for Metals, 1987.
9. Eiselstein, H. L. "Metallurgy of a Columbium-Hardened Nickel-Chromium-Iron Alloy." Advances in the Technology of Stainless Steels and Related Alloys. ASTM Special Technical Publication No. 369, 1965.
10. Baker, M. G. and D. J. Wood. "The Chemical Composition of Corrosion Products in Liquid Sodium." In Proceedings of the TMS-AIME Symposium on Chemical Aspects of Corrosion and Mass Transfer in Liquid Sodium, Detroit, October 19-20, 1971.

NASA
National Aeronautics and Space Administration

Report Documentation Page

1. Report No.	2. Government Accession No.	3. Recipient's Catalog No.
NASA CR-189120		

4. Title and Subtitle

Heat Pipe Fatigue Test Specimen:
Metallurgical Evaluation

5. Report Date
January 1992

6. Performing Organization Code

7. Author(s)

Steven E. Walak
Michael J. Cronin
Toni Grobstein

8. Performing Organization Report No.
91TR56

10. Work Unit No.
583-02-21

9. Performing Organization Name and Address

Mechanical Technology Incorporated
968 Albany-Shaker Road
Latham, New York 12110

11. Contract or Grant No.
NAS3-25463

13. Type of Report and Period Covered
Contractor Report - Topical
October 1990 - October 1991

12. Sponsoring Agency Name and Address

NASA-Lewis Research Center
21000 Brook Park Road
Cleveland, Ohio 44135

14. Sponsoring Agency Code

15. Supplementary Notes

Project Manager: James Dudenhoefer, NASA-Lewis Research Center, Cleveland, Ohio 44135;
Author: Toni Grobstein, NASA-Lewis Research Center, Cleveland, Ohio 44135

16. Abstract

An innovative creep/fatigue test was run to simulate the temperature, mechanical load and sodium corrosion conditions expected in a heat pipe designed to supply thermal energy to a Stirling cycle power converter. A sodium-charged Inconel 718 heat pipe with a Nickel 200 screen wick was operated for 1090 hr at temperatures between 950 K (1250°F) and 1050 K (1430°F) while being subjected to creep and fatigue loads in a servo-hydraulic testing machine.

After testing, the heat pipe was sectioned and examined using optical microscopy, scanning electron microscopy, and electron microprobe analysis with wavelength dispersive x-ray spectroscopy. The analysis concentrated on evaluating topographic, microstructural, and chemical changes in the sodium exposed surfaces of the heat pipe wall and wick. Surface changes in the evaporator, condenser, and adiabatic sections of the heat pipe were examined in an effort to correlate the changes with the expected sodium environment in the heat pipe. This report describes the setup, operating conditions, and analytical results of the sodium heat pipe fatigue test.

17. Key Words (Suggested by Author(s))	18. Distribution Statement
Heat Pipes, Nickel-Based Superalloys, Sodium, Corrosion, Creep, Fatigue, Inconel 718	Unclassified - Unlimited

19. Security Classif. (of this report)	20. Security Classif. (of this page)	21. No of pages	22. Price*
Unclassified	Unclassified	36	A03

*For sale by the National Technical Information Service, Springfield, Virginia 22161